Vibrational and structural properties of OH adsorbed on Pt(111)

Cite as: J. Chem. Phys. **111**, 11147 (1999); https://doi.org/10.1063/1.480472
Submitted: 11 May 1999 . Accepted: 27 September 1999 . Published Online: 09 December 1999

K. Bedürftig, S. Völkening, Y. Wang, J. Wintterlin, K. Jacobi, and G. Ertl

Vibrational and structural properties of OH adsorbed on Pt(111)

K. Bedürftig, S. Völkening, Y. Wang, J. Wintterlin, K. Jacobi,[a] and G. Ertl
Fritz-Haber-Institut der Max-Planck-Gesellschaft, Faradayweg 4-6, D-14195 Berlin, Germany

(Received 11 May 1999; accepted 27 September 1999)

OH species adsorbed on Pt(111) were studied in a combined investigation using scanning tunneling microscopy (STM) and high-resolution electron energy loss spectroscopy (HREELS). OH was formed by two different reactions, by reaction of H_2O with O, and as an intermediate in the reaction of O with hydrogen to H_2O. In both cases, two ordered OH phases were observed, a $(\sqrt{3}\times\sqrt{3})R30°$ and a (3×3) structure, for which models are proposed. Both structures have OH coverages of 2/3, and their formation is driven by hydrogen bond formation between the adparticles; the OH adsorption site is most likely on top. OH molecules at defects in the adlayer, in particular at island edges, are spectroscopically distinguishable and contribute significantly to the vibrational spectra in disordered OH layers. This is important for the water formation reaction, where the OH islands are small. The discrepancies between previous HREELS studies on OH can be explained by the different degree of order under the various formation conditions. © *1999 American Institute of Physics.* [S0021-9606(99)70148-0]

I. INTRODUCTION

Adsorbed hydroxyl plays an important role as reaction intermediate during the oxidation of hydrogen to water on Pt surfaces. However, published spectroscopic studies revealed quite conflicting data about the OH_{ad} species that occur under various reaction conditions. This fact, together with many other difficulties, prevented for a long time establishing a consistent picture of the mechanism of the hydrogen oxidation. For Pt(111), Fisher and Sexton reported[1] that OH_{ad} could be prepared by adsorption of H_2O on a layer of preadsorbed O atoms at 100 K and subsequent annealing to $T=150$ K, causing reaction with the oxygen atoms by

$$H_2O_{ad}+O_{ad}\rightarrow 2OH_{ad}. \quad (1)$$

Vibrational and electronic spectra indicated that a pure OH_{ad} layer was formed in this way. That OH_{ad} was not observed by x-ray photoemission spectroscopy[2] under conditions of the hydrogen oxidation indicated small concentrations of OH_{ad}, which seemed to suggest that it is only a short-lived intermediate. In a later study, Mitchell and White,[3] using high-resolution electron energy loss spectroscopy (HREELS), could actually detect OH_{ad} in an intermediate stage of the reaction, but the spectra were quite different from the Fisher/Sexton data. It was claimed that the OH_{ad} species under the conditions of the water formation is different from the one formed by reaction (1). A threefold hollow site was suggested, in contrast to the on-top bonded OH_{ad} resulting from the $H_2O_{ad}+O_{ad}$ reaction. Germer and Ho[4] also detected OH_{ad} during the water reaction, by recording fast HREEL spectra. However, the spectra were different from the Mitchell/White HREELS data under reaction conditions, but more similar to the Fisher/Sexton data for the $H_2O_{ad}+O_{ad}$ reaction; the reasons for these discrepancies remained unclear. Finally, photochemical dissociation of water[5] created an OH_{ad} species with different vibrational spectra than the one obtained by reaction (1), which was again interpreted as a threefold coordinated molecule.

Recently, based on a combined scanning tunneling microscopy (STM) and high-resolution electron energy loss spectroscopy (HREELS) study, we presented a new mechanism for the water formation reaction on Pt(111).[6] At $T<170$ K (the desorption maximum of H_2O, three steps occur,

$$\begin{aligned} &O_{ad}+H_{ad}\rightarrow OH_{ad} \ \text{(I)},\\ &OH_{ad}+H_{ad}\rightarrow H_2O_{ad} \ \text{(II)},\\ &H_2O_{ad}+O_{ad}\rightarrow 2OH_{ad} \ \text{(III)}. \end{aligned} \quad (2)$$

While (I) only starts the process, the bulk of the water is formed by cyclic repetition of (II) and (III), which makes the overall process autocatalytic and leads to the formation of reaction fronts. These contain most of the OH_{ad} present on the surface, which explains the small OH_{ad} concentration found by surface integrating techniques, and also many of the unusual observations in the context of this reaction.

However, the reported conclusions about the various observed OH_{ad} species[1,3–5] were still conflicting. Here we report a new, detailed investigation of this question by HREELS with improved resolution, in combination with STM. Additional information was obtained by temperature programmed desorption (TPD) and low energy electron diffraction (LEED). We arrive at a consistent picture which explains the existing discrepancies about this surface species by the different order of the OH_{ad} layer under the various formation conditions. In addition, models for the two ordered OH_{ad} structures that were discovered in this study will be proposed.

II. EXPERIMENT

The HREELS experiments were performed in an ultrahigh vacuum (UHV) apparatus (base pressure 3×10^{-11}

[a]Electronic mail: jacobi@fhi-berlin.mpg.de

mbar) consisting of two chambers connected by a valve.[7,8] The upper chamber contained an argon gun, a quadrupole mass spectrometer, and LEED optics; the lower chamber housed an HREEL spectrometer of the latest commercial Ibach design (Delta 0.5, SPECS, Germany). HREEL spectra were taken at an angle of 55° with respect to the surface normal in specular geometry at a resolution of $\leqslant 2$ meV. The scattering plane contains the $\overline{\Gamma M}$ azimuth. The electron beam energy was set to 2 eV.

The sample was mounted between *W* wires in narrow slits at its edges. It was heated by electron bombardment from the back side. The sample temperature was measured with a Ni–Cr/Ni thermocouple spot welded to the back of the crystal. It was cleaned by sputtering–oxidation–annealing cycles. Before each experiment the following procedure was carried out: (1) Annealing at 1370 K for 5 min, (2) Ar sputtering for 3 min at 500 eV and 5 μA, (3) flash annealing to 1370 K, (4) annealing at 1070 K for 3 min, (5) oxidation at 720 K with 1×10^{-7} mbar O_2 for 30 min, (6) annealing at 1370 K for 1 min. The cleanliness was checked by HREELS. The procedure removed all carbon and Pt oxide residues. Gas purities were 99.999% for H_2, 99.7% for D_2, 99.998% for $^{16}O_2$, 99.51% for $^{18}O_2$, and 99.0% for ^{18}O and D in $D_2{}^{18}O$. Additional purification of water and deuteriumoxide was achieved by repeated cycles of freezing, pumping, and thawing followed by vacuum distillation. We used a stainless steel UHV inlet system with liquid N_2 traps to condense any remaining water and avoided reduction valves for cleanliness. Dosing was performed by backfilling the preparation chamber while the sample was cooled to 85 K by liquid N_2. Coverages are given with respect to the number of substrate surface atoms and exposures in units of Langmuir (L)—1 $L=1.33\times10^{-6}$ mbar s. For the pressures of H_2 and D_2, correction factors of 2.27 and 2.86 were used, for the ionization gauge reading.

In the STM chamber, Auger electron spectroscopy (AES) and LEED optics were available for surface characterization. The sample holder in the STM was connected to a liquid He cryostat by a copper braid, which allowed us to cool the sample to 60 K. Higher temperatures were achieved by simultaneous irradiative heating of the sample from the back. The surface temperature was measured with a Ni–NiCr thermocouple spot welded to the back of the crystal; for the sample preparation in the STM chamber we refer to a previous publication.[9]

III. RESULTS AND DISCUSSION

A. TPD

On the basis of TPD experiments, Creighton and White[10] concluded that the stoichiometry of the $H_2O_{ad}+O_{ad}$ reaction is different from the 1:1 ratio of water and oxygen according to reaction (1). In these experiments a surface fully covered with a $(2\times2)^{18}O$ layer was exposed to $H_2{}^{16}O$ at 95 K and annealed; the resulting $^{18}OH_{ad}/^{16}OH_{ad}$ coverage ratio reflected the stoichiometry. At about 200 K, the OH molecules decayed again by the reverse $H_2O_{ad}+O_{ad}$ reaction so that the isotope ratio in the desorbing water measured the $^{18}OH_{ad}/^{16}OH_{ad}$ ratio. Because ^{18}O appeared in the detected water with a fraction of 0.31, independently of the amount of $H_2{}^{16}O$ adsorbed, a 2:1 ratio was concluded for the initial reaction of water with oxygen atoms. This result was reproduced in the present study, which revealed an ^{18}O fraction of 0.29. In agreement with the conclusions by Creighton and White, this leads to the equation

$$2H_2O_{ad}+O_{ad}\rightarrow 3OH_{ad}+H_{ad}. \tag{3}$$

As a consequence, the reaction of a perfect $(2\times2)O_{ad}$ layer $[\theta(O)=0.25]$ with water leads to a maximum OH_{ad} coverage of 0.75, instead of 0.5 resulting from a 1:1 stoichiometry. Equation (3) implies, furthermore, that additional hydrogen atoms must be present on the OH_{ad} covered surface. However, H_{ad} was not detected by HREELS, which has to be attributed to the low loss intensities measured in spectra of pure H_{ad} layers,[11] nor was it resolved by STM. Adsorption of larger quantities of additional hydrogen atoms in layers of other adsorbates is, however, not unusual, and has been reported, e.g., for Cs on Ru(0001)[12] and for oxygen atoms and molecules on Pt(111).[13] We emphasize that the unexpected stoichiometry of the $H_2O_{ad}+O_{ad}$ reaction does not invalidate the water formation mechanism (2), as already mentioned in Ref. 6, although the reaction enters the sequence as step III. In the simplified scheme (2), a cycle consisting of steps II and III doubles the number of OH_{ad} molecules, whereas with the 2:1 stoichiometry of reaction (3) the multiplication factor is 1.5. The process is hence still autocatalytic.

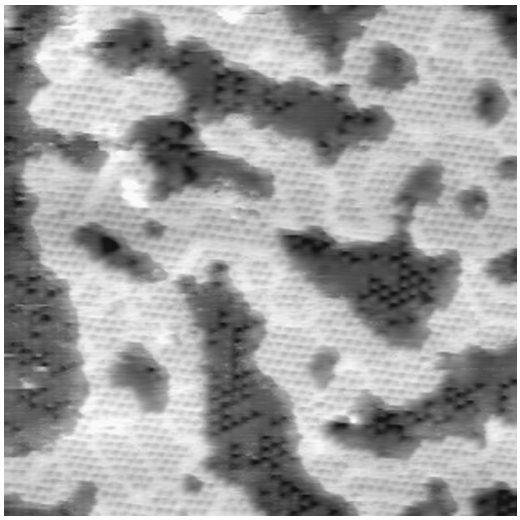

FIG. 1. (a) STM image of an OH_{ad} layer on Pt(111), formed by the reaction of a (2×2)-O layer $[\theta(O)\approx0.15]$ with 0.5 L H_2O at 130 K. Tunneling parameters were −0.55 V (sample potential), 0.8 nA, image size 220×220 Å^2.

B. STM and LEED

To our knowledge, LEED studies of OH_{ad} on Pt(111) have so far not been reported. Using LEED we find that, upon H_2O adsorption on the $(2\times2)O_{ad}$ structure at $T\geqslant150$ K, the (2×2) spots gradually disappear and diffraction spots of a $(\sqrt{3}\times\sqrt{3})R30°$ structure emerge. In both UHV systems, HREELS and STM, this LEED pattern was observed under the same preparation conditions. The same transition was observed by STM. Figure 1 shows an STM image, recorded in an intermediate stage of an experiment in

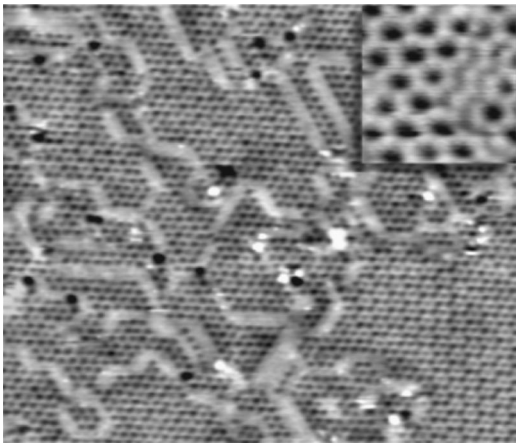

FIG. 2. STM image of an OH_{ad} layer on Pt(111), formed by adsorption of 2 L H_2O on a (2×2)-O layer at 123 K and short annealing at 170 K. Tunneling parameters were -0.55 V, 0.17 nA, 220×220 Å^2. Inset: Detail of a boundary between translational domains of the $(3\times3)/(\sqrt{3}\times\sqrt{3})R30°$-OH structure; -0.01 V, 27 nA, 22×25 Å^2.

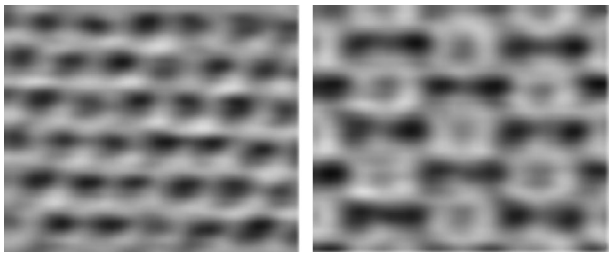

FIG. 3. Details of areas with (a) the Pt(111)-$(\sqrt{3}\times\sqrt{3})R30°$-OH and (b) the Pt(111)-$(3\times3)$-OH structure from the measurement shown in Fig. 2. -0.5 V, 0.17 nA, 34×25 Å^2. Slight deviations from hexagonal symmetry in (a) are most likely caused by an asymmetric tip.

which a surface covered with oxygen $[\theta(O)\approx0.15]$ was exposed to 0.5 L of H_2O at 130 K. Large parts of the surface are covered by a bright layer; the dark patches are areas of bare platinum with some oxygen atoms. The O_{ad} atoms are imaged dark, which is typical for oxygen atoms on metal surfaces.[9] The partial hexagonal order represents the $(2\times2)O_{ad}$ structure, small clusters of which have not yet reacted. The bright area displays a hexagonal structure, too, but the smaller lattice constant and the rotation of the lattice with respect to the (2×2) structure mark a $(\sqrt{3}\times\sqrt{3})R30°$ structure. There are several pieces of evidence that this structure is composed of OH_{ad} and does not contain H_2O_{ad}: The various ice structures formed by water on Pt(111) that were studied in detail by Morgenstern[14] are clearly different; at $T\leqslant80$ K, where the $H_2O_{ad}+O_{ad}$ reaction does not take place, the structure seen in Fig. 1 does not occur; during the hydrogen oxidation, when at some stage OH_{ad} and H_2O_{ad} coexist, the two species could be clearly discriminated by their different structures, island shapes, and mobilities; and, most importantly, HREELS does not show water peaks under these conditions.

If water was adsorbed on a surface fully covered with oxygen atoms $[\theta(O)=0.25]$, STM images like the one shown in Fig. 2 were obtained. Here 2 L of H_2O were adsorbed on the $(2\times2)O_{ad}$ covered surface at 123 K, followed by short annealing at 170 K. In a previous HREELS and photoelectron spectroscopy study,[15] it was shown that under these conditions H_2O reacts completely to OH_{ad}, and excess water desorbs during the annealing [the decay of OH_{ad} and subsequent desorption of water by the reverse reaction (3) occurs only at higher temperatures, at around 205 K[10]]. The surface (Fig. 2) is then completely covered by an OH_{ad} layer, part of which displays the simple hexagonal pattern of the $(\sqrt{3}\times\sqrt{3})R30°$ structure; the bright lines are domain boundaries. In some domains the hexagonal structure has rearranged into a honeycomb pattern (most clearly at the larger domain at the right-hand side of the image) which represents a (3×3) structure. Except for the different periodicity, this structure very much resembles the $(\sqrt{3}\times\sqrt{3})R30°$ structure, and in some domains there is a smooth transition between the $(\sqrt{3}\times\sqrt{3})R30°$ and the (3×3) structures.

The close similarity of the two structures becomes evident also in close-up images (Fig. 3). The $(\sqrt{3}\times\sqrt{3})R30°$ structure appears as a hexagonal pattern of identical dark dots, which become inequivalent in the (3×3) structure; one out of three dots is smaller, two dots are wider than in the $(\sqrt{3}\times\sqrt{3})R30°$ structure. We take this likeness as evidence of only local rearrangements of OH_{ad} molecules about their positions so that the OH_{ad} densities are equal in the two structures. The (3×3) structure is thermodynamically more stable than the $(\sqrt{3}\times\sqrt{3})R30°$ structure which follows from the higher portion of the (3×3) phase at higher reaction temperatures, and from the observation that the $(\sqrt{3}\times\sqrt{3})R30°$ structure is transformed into the (3×3) structure by annealing. Spots of a (3×3) pattern were not detected by LEED, which will be explained later.

Figure 2 shows that the reaction of a full $(2\times2)O_{ad}$ layer with water results in a completely OH_{ad} covered surface, which, according to reaction (3), corresponds to a maximum OH_{ad} coverage of 0.75. Because a fully developed $(\sqrt{3}\times\sqrt{3})R30°$ structure must have an OH_{ad} coverage of a multiple of 1/3, and because the (3×3) structure has the same OH_{ad} density, the actual coverage is obviously 0.67. The difference between 0.75 and 0.67 may be accounted for, if either the initial $(2\times2)O_{ad}$ phase exhibited some vacancies, or if the domain boundaries seen in Fig. 2 accommodate additional OH_{ad} molecules (''heavy walls''). The latter explanation is supported by images recorded with improved resolution (inset of Fig. 2), which demonstrate that the domain boundaries, the brighter stripes in Fig. 2, are actually formed by (1×1) structure elements, corresponding to a local coverage of 1.0. The $(\sqrt{3}\times\sqrt{3})R30°$ unit cell must therefore contain two OH_{ad} molecules. The same conclusion was reached at by STM experiments (not shown here), in which OH_{ad} layers were reacted with hydrogen to water which has a known coverage.

Based on the above information we propose the following models for the $(\sqrt{3}\times\sqrt{3})R30°$ and (3×3) structures (Fig. 4). The hydroxyl molecules are assumed to occupy on-top sites, because the intense OH bending mode in HREELS indicates that the OH molecule must be tilted from the surface normal. This involves sp^3 hybridization of the oxygen atom which favors the on-top site. A threefold hollow site of the OH_{ad} would require sp hybridization of the oxygen atom

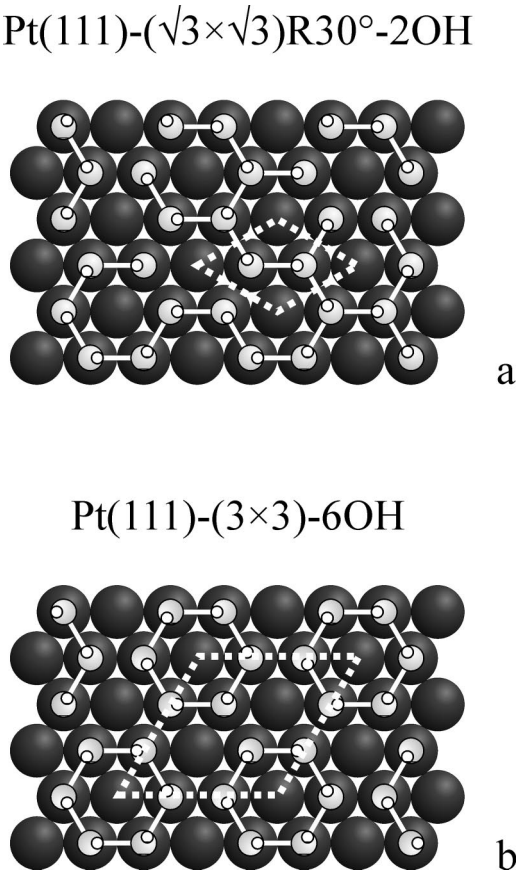

FIG. 4. (a) Models of the Pt(111)-($\sqrt{3}\times\sqrt{3}$)$R30°$-OH and of (b) the Pt(111)-(3×3)-OH structure. Bars indicate hydrogen bonds, the broken lines the unit cells of the two structures.

to allow sufficient overlap of the oxygen *p*-orbitals with the platinum *s*- and *d*-inplane orbitals. The resulting Pt–O–H bond angle of 180° would make the OH-bending mode invisible in specular HREEL spectra, which contrasts the experimental finding. Recent density functional calculations on the adsorption of a hydroxyl group on a Pt_6 cluster also favored the on-top site.[16] For SH_{ad} on Au(111) and Ag(111) surfaces, *ab initio* calculations also predict the on-top site, if the molecule is tilted with respect to the normal.[17] A tilted geometry is required also in order that the OH_{ad} molecules can form hydrogen bonds with each other, which we believe is the driving force for the formation of these structures. For the ($\sqrt{3}\times\sqrt{3}$)$R30°$ structure, we assume random orientations of the hydrogen bonds, which possibly fluctuate in time, in order to account for the hexagonal symmetry of the structure seen by STM.

A (3×3) structure can then be understood by assuming that the hydrogen bonds lock in, which causes the formation of six-membered OH_{ad} rings. This explains the honeycomb pattern and the similar appearances of the two structures in STM. The absence of a (3×3) LEED pattern is attributed to the small scattering cross section of hydrogen for electrons, because the ($\sqrt{3}\times\sqrt{3}$)$R30°$ and the (3×3) structures differ only by the orientations of the hydrogen atoms. The positions of the O atoms, which mainly cause the overlayer scattering spots in LEED, remain unchanged. Circular arrangements with hydrogen bonds are a very attractive possibility.

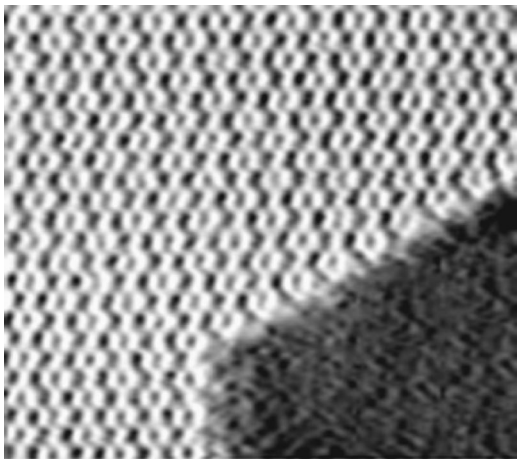

FIG. 5. STM image of a (3×3)OH_{ad} island edge. The surface was prepared by annealing of the OH_{ad} layer from Fig. 1 for 5 min at 160 K. $T = 130$ K; −0.5 V, 2.5 nA; 115×100 Å^2. Similarly as in Fig. 3, slight deviations from hexagonal symmetry are most likely caused by an asymmetric tip.

Ab initio calculations of water[18] showed that hydrogen bonds are not additive, but become stronger with additional attached water molecules, from which it was predicted that chains, and in particular rings of water molecules, should be preferred. For certain OH-containing organic molecules, so-called *homodromic* circles, with all hydrogen bonds running in the same directions, have actually been observed.[19,20] That circles are particularly stable also in the present case is supported by the greater thermodynamic stability of the (3×3) structure and the shape of (3×3) island edges which are often formed by intact six-membered rings of the honeycomb pattern (Fig. 5). LEED-I(V) investigations are in progress to test these models.[21] [We do not have information about the location of the additional hydrogen atoms bonded to the metal surface that must be present according to reaction (3).]

The same two structures were observed also under the conditions of the $H_{ad}+O_{ad}$ to water reaction (see Ref. 6), indicating that the same OH_{ad} species is formed as an intermediate of this reaction. Figure 6 shows an example of an image that was recorded during the reaction between O and H at 133 K, showing bright islands with a ($\sqrt{3}\times\sqrt{3}$)$R30°$ structure and dark areas with the (2×2)O_{ad} structure. That the hydroxyl islands are relatively small and display irregular borders results from the reduced mobility of the hydroxyl molecules at this low temperature. Well-ordered OH_{ad} islands as seen in Fig. 5 were obtained by annealing at higher temperatures for several minutes.

C. HREELS

Figure 7 shows HREEL spectra of $^{16}OH_{ad}$ and $^{18}OD_{ad}$. These were recorded after exposing the Pt surface to 10 L $^{16}O_2$ ($^{18}O_2$) at 90 K and annealing at 205 K for 30 s in order to prepare the (2×2) phase of atomic oxygen. Then 1 L of $H_2{}^{16}O$ ($D_2{}^{18}O$) was dosed and annealed at 155 K for 300 s to obtain a well-ordered OH_{ad} overlayer. All observed loss energies, their assignments, isotope shifts, and an explanation of the abbreviations are given in Table I. In addition to the OD related losses, the OD spectrum shows OH features at

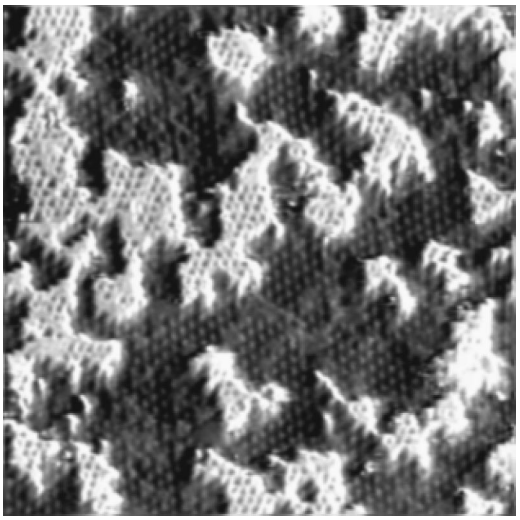

FIG. 6. STM image of the (2×2)-O covered Pt(111) surface after exposure of 7 L H_2 at 133 K. Tunneling parameters were 0.5 V, 0.8 nA; 170×170 Å^2. The bright areas correspond to OH_{ad} islands, the dark areas with the hexagonal pattern to the (2×2)-O_{ad} structure.

430, 127, and 115 meV which are caused by hydrogen exchange with coadsorbed hydrogen from the residual gas during the OD formation.

The ν(O–H), $\delta_{\parallel 1}$(OH), and ν(Pt–OH) modes at 430, 127, and 54 meV have been identified in previous studies.[1,22] In addition, Gilarowski *et al.*[5] recently reported the observation of the $\delta_{\parallel 3}$(OH)- and the $T_{\parallel}$(Pt–OH) mode at 102 and 43 meV. They also observed a loss at 29 meV but did not give an assignment. Figure 7 shows a third weak mode at 113 meV. Its isotope shift of 1.36 with respect to the loss in the ^{18}OD spectrum at 84 meV indicates a third bending mode. An explanation will be given below. In the range between 260 to 140 meV, two losses with intensities comparable to that of the ν(O–H) mode are resolved at 254 and 182 meV.

1. The O–H stretching mode ν(O–H)

If one compares the energy of the ν(O–H) mode (431 meV) to that of the ν(O–H) modes of free (458 meV) and hydrogen-bonded H atoms in H_2O_{ad} on Pt(111) (423 meV;

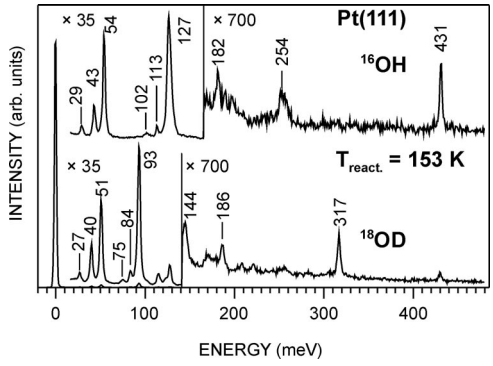

FIG. 7. HREEL spectra of a full layer of ^{16}OH(^{18}OD) on Pt(111) prepared by annealing of a coadsorbed (2×2)-^{16}O(^{18}O) layer and 1.0 L $H_2{}^{16}O(D_2{}^{18}O)$ at 155 K for 300 s. Primary energy of the electrons was 2 eV. Angle of incidence was 55° with respect to the surface normal, specular geometry.

TABLE I. Vibrational frequencies of hydroxyl on Pt(111) at 85 K. ν=stretch, δ=bend, T=translation, $\parallel/\perp$=motion parallel/perpendicular to the plane formed by the OH bond and the surface normal.

		^{16}OH (meV)	^{18}OD (meV)	Isotope shift
Stretching	ν(O–H)	431.0	316.9	1.36
Bending	$\delta_{\perp}^{(2)}$(OH)	254.1	186.2	1.37
	$\delta_{\parallel 1}$(OH)+$\nu_{\perp}$(Pt–OH)	181.5	144.3	1.26
	$\delta_{\parallel 1}$(OH)	126.8	93.1	1.36
	$\delta_{\parallel 2}$(OH)	113.4	83.7	1.36
	$\delta_{\parallel 3}$(OH)	101.8	75.1	1.36
Pt–OH stretching	ν(Pt–OH)	54.0	50.7	1.07
Hindered translation	$T_{\parallel}$(Pt–OH)	43.0	39.9	1.08
	$T_{\perp}$(Pt–OH)	29.0	26.7	1.09

own measurements, same energies as on Pt(100)[23]), it is obvious that OH_{ad} forms hydrogen bonds, because the energy of the O–H stretching is close to that of hydrogen-bonded H atoms of H_2O_{ad}. This is further supported by the energies of the ν(O–H) modes of (1) free OH radicals of 450 meV,[24] (2) of non-hydrogen-bonded adsorbed OH on Si(100) of 463 meV,[25] and (3) of non-hydrogen-bonded adsorbed KOH on Pt(111) of 456 meV.[26] We conclude that the redshift of about 20 meV with respect to non-hydrogen-bonded OH molecules evidences that the OH_{ad} on Pt(111) forms hydrogen bonds. Another example of OH_{ad} forming hydrogen bonds was found for Pd(100). The stretching frequency of 406 meV, which is even lower than that of the ν(O–H) mode of hydrogen-bonded H_2O_{ad} (422 meV),[27] indicates, however, an additional contribution from a different adsorption site. For Pd(100) it was shown[27] that OH_{ad} adsorbs on a two-fold bridge site. The fact that OH_{ad} is tilted toward the surface, as indicated by the strong dipole active bending mode ($\delta_{\parallel 1}$(OH) at 127 and 93 meV for ^{16}OH, ^{18}OD, see Fig. 7), makes it almost impossible to avoid the formation of hydrogen bonds considering the fact that in both structures hydroxyl molecules sit on nearest-neighbor sites, as illustrated in Fig. 4. An assumed tilt angle of 104° results in a hydrogen bond length of 1.9 Å for an O–H bond length of 1 Å. This compares well with the value for bulk ice of 1.76 Å.[28]

2. The OH bending modes δ(OH)

The loss at 127 meV had already been assigned to a bending mode of adsorbed hydroxyl.[1,5,22] However, as mentioned above, two further modes at 102 and 113 meV were observed here. The isotope shifts of 1.36 with respect to the corresponding losses in the ^{18}OD spectrum at 75 and 84 meV indicate H-related modes. Because the energies of these two modes are only slightly different from the bending mode at 127 meV, it is likely that these modes are bending modes as well. We can exclude coadsorbed H_2O_{ad} as an origin for these losses, because the HREEL spectra of OH_{ad}/H_2O_{ad} coadsorbates, which were prepared by dosing of H_2O on different coverages of OH_{ad} (not shown here), are different. Furthermore, coadsorption of water does not influence the intensity of these losses. The mode at 102 meV was also reported by Gilarowski *et al.*[5] They concluded that OH adsorbs at threefold hollow sites with a tilt angle of 15° relative

to the surface normal, which was supported by calculations based on a central force model. This result is not in agreement with the prediction of Fisher and Sexton[1] of a Pt–O–H angle of 100–120° (derived from considerations about the O atom hybridization) corresponding to a tilt angle of the hydrogen of 60–80° from the surface normal. The assignment of the two bending modes at 127 and 102 meV in Ref. 5 raises some additional questions. If the mode at 102 meV is actually assigned to the bending parallel to the plane formed by the OH bond, and the surface normal (dipole active) and the loss at 127 meV to the bending perpendicular to this plane (dipole forbidden), it is surprising that the dipole-forbidden mode dominates the spectrum and that the intensity of the dipole active mode is about five times smaller.

The new finding of a third bending mode at 113 meV (Fig. 6) demands a new interpretation. It is impossible that three bending modes are caused by one OH_{ad} configuration. Theoretically, two bending modes are possible, but only one of them will be dipole active if the adsorbed molecule is tilted. We conclude, therefore, that the losses at 113 and 102 meV are caused by structurally modified hydroxyl molecules which are hydrogen bond acceptors but not donors, which means that they have non-hydrogen-bonded hydrogen atoms. These exist, e.g., at the perimeters of OH_{ad} islands, where always some of the OH molecules will be tilted away from the island so that the respective hydrogen atoms cannot form hydrogen bonds. Other possibilities for OH_{ad} molecules with unsaturated hydrogen bonds exist at domain boundaries of the $(\sqrt{3}\times\sqrt{3})R30°$ and (3×3) structures and also for molecules in the interior of $(\sqrt{3}\times\sqrt{3})R30°$ islands. According to the structure model (Fig. 4), many of the OH molecules can be accommodated in hydrogen-bonded chains, but there will always be some ''open ends.'' The comparison of the bending mode energies of hydrogen-bonded OH_{ad} on Pd(100) of 116 meV[27] with that of non-hydrogen-bonded OH_{ad} on Si(100) of 103 meV[25] and non-hydrogen-bonded KOH_{ad} on Pt(111) of 96 meV[26] supports this assignment. Hydrogen bonding obviously strengthens the bending mode. The two losses at 102 and 113 meV are assigned to species with two and one next-neighbor molecules, respectively. This modification in the neighborhood of OH_{ad} without a variation of the adsorption site explains why only the energy of the bending mode and not of the other modes is changed. A change of the energy of the ν(O–H) mode is expected, because hydrogen bonding weakens the O–H stretching mode. For hydroxyl molecules in different adsorption sites, one would expect to find also different energies, e.g., for the corresponding ν(Pt–OH) mode. The corresponding ν(O–H) mode for nondonor OH molecules is expected at ~460 meV but is not observable in the HREEL spectra because of the generally lower intensity in the ν(O–H) region.

That the OH bending mode is actually affected by variations of the individual hydrogen bond arrangements follows from HREEL spectra of OH_{ad}/O_{ad} coadsorbates, which were prepared like the above OH_{ad} overlayers except that smaller quantities of H_2O_{ad} were dosed. Figure 8 shows spectra recorded after dosing 0.1 L of $H_2{}^{16}O/D_2{}^{18}O$ on the (2×2)-$^{16}O/^{18}O$ structure and annealing at 155 K for 300 s. The presence of a (2×2) and a $(\sqrt{3}\times\sqrt{3})R30°$ pattern in LEED

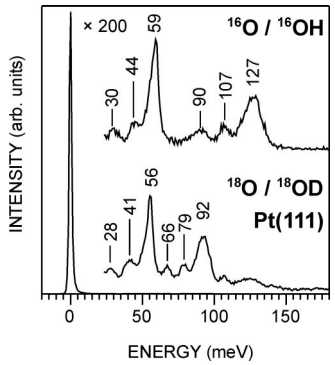

FIG. 8. HREEL spectra from a $^{16}OH/^{16}O(^{18}OD/^{18}O)$ coadsorbate on Pt(111) prepared by annealing of a coadsorbed layer of (2×2)-$^{16}O(^{18}O)$ and 0.1 L $H_2{}^{16}O(D_2{}^{18}O)$ at 155 K for 300 s. Parameters as in Fig. 7.

indicates that oxygen and hydroxyl islands are present on the platinum surface at the same time. The dominating loss is the Pt–O stretching mode at 59 and 56 meV, respectively, which is due to excess O_{ad}. These peaks show shoulders at the low-energy sides corresponding to ν(Pt–OH) [ν(Pt–OD)]. The position of the $\delta_{\parallel1}$(OH) bending mode at 127 meV is almost unchanged, although the full width at half maximum (FWHM) is drastically increased, which results from disorder of the hydroxyl layer caused by the reduced mobility of the OH molecules in the presence of O_{ad}. The $\delta_{\parallel2}$(OH) bending mode shifts to lower energies by a factor 1.06 and the $\delta_{\parallel3}$(OH) mode by a factor 1.14. The intensities of the $\delta_{\parallel2}$(OH) and $\delta_{\parallel3}$(OH) modes with respect to the $\delta_{\parallel1}$(OH) mode are larger by a factor of about four, indicating smaller islands with a larger relative amount of perimeter hydroxyl molecules in a different surrounding compared to the situation of Fig. 7. Figure 8 demonstrates that the coadsorbed oxygen only influences the position of two of the three bending modes. The redshift of two modes and the unchanged position of the third mode can only be explained in terms of interactions between the boundaries of oxygen and hydroxyl islands. If OH_{ad} in on-top sites at the perimeters of hydroxyl islands forms hydrogen bonds with neighboring oxygen atoms in threefold hollow sites, it has to tilt more strongly. Whereas the formation of hydrogen bonds should increase the bending mode energy, tilting toward the surface could decrease it due to the change in bonding geometry. The lower energy shows that the tilting compensates for the effect of the hydrogen bonding, which is also expected to be weak in this case because of the larger distance between OH_{ad} and O_{ad}. Because the perimeter hydroxyls are minority species, the corresponding O–H stretching frequencies were not seen (as mentioned above) which will expected to be at energies higher than 431 meV.

3. Multiple losses and overtones

The loss at 254 meV (Fig. 7) is interpreted as the dipole-active overtone of a bending perpendicular to the plane formed by the OH bond and the surface normal. The fundamental, the $\delta_{\perp}$(OH) mode, is not dipole active and is not observed in specular direction. From the energy of its dipole-active overtone it should be at around 130 meV, which

means that the bending modes parallel and perpendicular to the plane formed by the OH bond and the surface normal have almost the same energy. This is what one expects for an hydroxyl adsorbed in the on-top position. An assignment as double loss of the $\delta_{\parallel 1}(\mathrm{OH})$ mode is implausible because in this case the overtone $\delta_{\parallel 1}{}^{(2)}(\mathrm{OH})$ should be observable as well, at somewhat lower energy and with higher intensity than the double loss,[29] which is not the case. The loss at 182 meV is attributed to the combination of the two most intense modes, the $\delta_{\parallel 1}(\mathrm{OH})$ mode and the $\nu_{\perp}(\mathrm{Pt{-}OH})$ mode.

4. Pt–OH stretching and translational modes

The assignment of the remaining three losses is straightforward. The loss at 54 meV is caused by the Pt–OH stretch[1,5,22] in agreement with the isotope shift of 1.07 for ^{18}OD. Vibrational modes that correspond to the motion of the whole molecule with respect to the surface should show an isotope shift of 1.09 if ^{16}OH is substituted by ^{18}OD. Hence OH_{ad} is also the origin of the losses at 43 and 29 meV, as indicated by the isotope shifts for ^{18}OD of $\sim$1.08. The loss at 43 meV is assigned to a hindered translation.[5] The surprisingly high energy of this hindered translation $T_{\parallel}(\mathrm{Pt{-}OH})$ can be explained by mixing of this mode with the $\delta_{\parallel 1}(\mathrm{OH})$ bending that is caused by the tilting of the OH_{ad} molecule.[30] This leads to the result that the $T_{\parallel}(\mathrm{Pt{-}OH})$ is a hindered translation in the plane formed by the OH bond and the surface normal. The second hindered translation, the $T_{\perp}(\mathrm{Pt{-}OH})$ mode, is in a direction perpendicular to this plane. Therefore it is not dipole active and the observed intensity is about three times smaller. That it is detected in the HREEL spectrum in specular geometry might be caused by coupling with other dipole-active modes and possibly also by a contribution from impact scattering. A hindered translation in the direction defined above will weaken the hydrogen bond and might lead to a change in the tilting angle. Hence this mode couples with the bending mode.

5. The OH bending mode in the H_2O formation reaction

Finally, we turn to the transient OH species that is formed during the H_2O formation reaction. As already mentioned, there are inconsistencies in the literature concerning the OH bending mode and its evolution during the water formation reaction. Mitchel and White[3] identified an intermediate which was interpreted as hydroxyl although it had vibrational properties different from OH_{ad} formed by the $O_{ad}+H_2O_{ad}$ reaction. The lower energy of the bending mode (99 meV) was believed to be due to adsorption in threefold hollow sites and the absence of the $\nu(\mathrm{O{-}H})$ mode due to the low hydroxyl coverage. Germer and Ho[4] observed the bending mode at 120 meV, almost at the same energy as in Fisher and Sexton's[1] work (126 meV) and used it as an indicator for θ_{OH} during the water formation reaction. Because of a resolution of 12 meV at that time, the $\nu(\mathrm{Pt{-}OH})$ mode was not resolved in the presence of O_{ad} and H_2O_{ad}.

Figure 9 shows HREEL spectra recorded after quenching the $O_{ad}+H_{ad}$ reaction that was performed under several different reaction conditions. In addition to OH-related

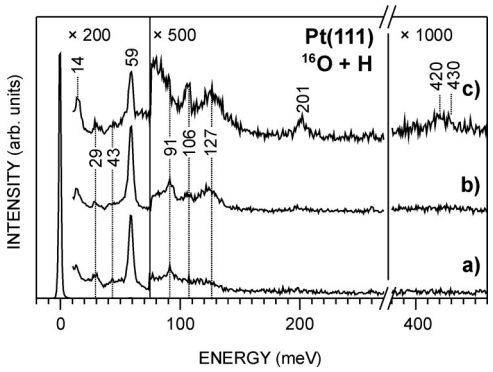

FIG. 9. HREEL spectra from Pt(111) recorded after (a) exposure of 7 L of H_2 on the (2×2)-^{16}O structure at 128 K and quenching to 85 K, (b) exposure of 3 L of H_2 on the (2×2)-^{16}O structure at 146 K and quenching to 85 K, (c) exposure of 9 L of H_2 on the (2×2)-^{16}O structure at 133 K and quenching to 85 K. Parameters as in Fig. 6.

modes—the weak hindered translations at 29 and 43 meV, the bending modes at 91, 106, and 127 meV—the spectra show one oxygen-related mode at 59 meV and five water-related modes: the hindered translations at 14 meV that were observed here for the first time (discussed in detail in a forthcoming paper[31]) and at $\sim$30 meV as a shoulder at the high energy side of the $T_{\perp}(\mathrm{Pt{-}OH})$ mode, the librations at 60–90 meV and the scissors mode at 201 meV (curve c), and finally the $\nu(\mathrm{O{-}H})$ mode of hydrogen-bonded water molecules. In all cases OH_{ad} is present on the surface. Based on the interpretation of the pure OH_{ad} phase, all modes can be easily assigned. In curve a there are almost only hydroxyl molecules at the borders of oxygen islands, as indicated by a single bending mode at 91 meV. In curve b, after reaction at a higher temperature but smaller hydrogen exposure, roughly the same amount of O_{ad} remains on the surface, as indicated by the $\nu(\mathrm{P{-}O})$ mode at 59 meV, but all of the three OH species with different hydrogen bonds are present. The three bending modes appear at almost the same energies as in Fig. 8 but with different intensity ratios. This is reasonable if the hydroxyl islands are smaller. Curve c shows a situation comparable to that in the spectra of Germer and Ho.[4] The bending mode of OH_{ad} inside of the islands is easily seen, but the other two bending modes are also resolved, although the $\delta_{\parallel 3}(\mathrm{OH})$ mode is superimposed by the water librations.

The discrepancies between the measurements of Germer and Ho[4] and Mitchell and White[3] become resolved if one compares curves a and c. The single loss at energies around 91 meV in curve a indicates an earlier stage of the reaction, where no OH_{ad} islands have formed yet, as indicated by the absence of a loss at 127 meV. Curve c describes a state with larger $\theta(\mathrm{OH})$, where small hydroxyl islands have evolved. STM measurements of the reaction under comparable conditions (Fig. 6) show exactly this picture. The slightly different energies of our measurements compared with earlier work—Germer and Ho observed the OH bending at 120 meV (our work 127 meV) and Mitchell and White at 99 meV (our work 91 meV)—might be caused by intensity and resolution problems in older HREEL spectrometers. That we find the same energies independently of the type of the reaction ($H_2O_{ad}+O_{ad}$ or hydrogen oxidation) by which OH_{ad} is being

formed, leads to the conclusion that the hydroxyl species is always the same. The spectroscopic variations can be fully understood from the different surroundings and island sizes that influence intensity ratios and the FWHM of the three observable bending modes.

IV. CONCLUSION

In conclusion, we arrive at a new interpretation of the properties of OH_{ad} on Pt(111). The investigation comprised OH_{ad} layers prepared under various temperature and coverage conditions, by reaction of O_{ad} with H_2O_{ad} and by reaction of O_{ad} with hydrogen.

The HREEL spectra obtained display complex changes depending on the formation conditions, which reflects the variations between previous studies. However, due to improved resolution, if compared with the older work, all loss peaks can be assigned. A consistent picture is obtained assuming that OH_{ad} adopts a single adsorption state with an on-top position on the Pt surface atoms, a tilting with respect to the surface normal, and hydrogen bonds to neighboring hydroxyl molecules.

STM images show that the OH_{ad} layer forms ordered phases with $(\sqrt{3}\times\sqrt{3})R30°$ or (3×3) periodicities. According to TPD data, both structures exhibit local OH_{ad} coverages of 2/3. With this information, models for the two structures have been developed using a single OH_{ad} adsorption site and assuming random or circular hydrogen bonds between the hydroxyl molecules. The circumstances under which the OH_{ad} layer is formed affect the island sizes and the area ratio and order of the $(\sqrt{3}\times\sqrt{3})R30°$ and (3×3) covered areas.

The spectroscopic variations observed here and found in the literature can be explained by effects of the hydrogen bonds. OH_{ad} molecules not ''saturated'' by hydrogen bonds, which occur in the $(\sqrt{3}\times\sqrt{3})R30°$ structure, at defects of OH_{ad} islands, and at their edges, can explain additional loss peaks. Further spectral changes occur, if the OH islands are surrounded by O_{ad} atoms, by the formation of hydrogen bonds between OH_{ad} molecules and oxygen atoms. The spectroscopic variations can therefore be understood as an effect of the order of the OH_{ad} layer, which is a function of the different formation conditions.

In this way a coherent explanation emerges for the discrepancies between previous studies. In particular the apparent differences between the OH_{ad} species formed under the conditions of the $H_2O_{ad}+O_{ad}$ reaction and the hydrogen oxidation are removed. This result lends further credit to our model of the hydrogen oxidation,[6] in which OH_{ad} is an essential ingredient.

ACKNOWLEDGMENTS

We thank H. Hartl and A. P. Seitsonen for helpful discussions and P. Geng for skillful technical assistance.

[1] G. B. Fisher and B. A. Sexton, Phys. Rev. Lett. **77**, 683 (1980).
[2] G. B. Fisher, J. L. Gland, and S. J. Schmieg, J. Vac. Sci. Technol. **20**, 518 (1982).
[3] G. E. Mitchell and J. M. White, Chem. Phys. Lett. **135**, 84 (1987).
[4] T. A. Germer and W. Ho, Chem. Phys. Lett. **163**, 449 (1989).
[5] G. Gilarowski, W. Erley, and H. Ibach, Surf. Sci. **351**, 156 (1996).
[6] S. Völkening, K. Bedürftig, K. Jacobi, J. Wintterlin, and G. Ertl, Phys. Rev. Lett. **83**, 2672 (1999).
[7] M. Gruyters and K. Jacobi, J. Electron Spectrosc. Relat. Phenom. **64–65**, 591 (1993).
[8] H. Shi, K. Jacobi, and G. Ertl, J. Chem. Phys. **99**, 9248 (1993).
[9] J. Wintterlin, R. Schuster, and G. Ertl, Phys. Rev. Lett. **77**, 123 (1996).
[10] J. R. Creighton and J. M. White, Surf. Sci. **122**, L648 (1982).
[11] K. Bedürftig, Y. Wang, K. Jacobi, and G. Ertl (in preparation).
[12] H. Shi, P. Geng, and K. Jacobi, Surf. Sci. **315**, 1 (1994).
[13] A. T. Capitano, A. M. Gabelnick, and J. L. Gland, Surf. Sci. **419**, 104 (1999).
[14] M. Morgenstern, J. Müller, T. Michely, and G. Comsa, Z. Phys. Chem. **198**, 43 (1997).
[15] F. T. Wagner and T. E. Moylan, Surf. Sci. **191**, 121 (1987).
[16] A. Fahmi and R. A. van Santen, Z. Phys. Chem. **197**, 203 (1996).
[17] H. Sellers, A. Ulman, Y. Shnidman, and J. E. Eilers, J. Am. Chem. Soc. **115**, 9389 (1993).
[18] J. Del Bene and J. A. Pople, J. Chem. Phys. **52**, 4858 (1970).
[19] G. A. Jeffrey and A. Robbins, Acta Crystallogr., Sect. B: Struct. Crystallogr. Cryst. Chem. **34**, 3817 (1978).
[20] W. Saenger, Nature (London) **279**, 343 (1979).
[21] J. Zhu, K. Bedürftig, K. Jacobi, H. Over, and G. Ertl (in preparation).
[22] A. V. Melo, W. E. O'Grady, G. S. Chottiner, and R. W. Hoffman, Appl. Surf. Sci. **21**, 160 (1985).
[23] H. Ibach and S. Lehwald, Surf. Sci. **91**, 187 (1980).
[24] M. W. Urban, *Vibrational Spectroscopy of Molecules and Macromolecules on Surfaces* (Wiley, New York, 1993), p. 138.
[25] H. Ibach, H. Wagner, and D. Bruchmann, Solid State Commun. **42**, 457 (1982).
[26] C. Klünker, C. Steimer, J. B. Hannon, M. Giesen, and H. Ibach, Surf. Sci. **420**, 25 (1999).
[27] E. M. Stuve, S. W. Jorgensen, and R. J. Madix, Surf. Sci. **146**, 179 (1984).
[28] A. F. Hollemann and N. Wiberg, Lehrbuch der anorganischen Chemie, 91-100 ed. (Walter de Gruyter, Berlin, 1985), p. 282.
[29] S. Lehwald, H. Ibach, and H. Steininger, Surf. Sci. **117**, 342 (1982).
[30] H. Ibach and D. L. Mills, *Electron Energy Loss Spectroscopy and Surface Vibrations* (Academic, New York, 1982), p. 184.
[31] K. Bedürftig, Y. Wang, K. Jacobi, and G. Ertl (in preparation).